


Numerical investigation of the heat pump system

Sánta Róbert¹  · László Garbai² · Igor Fürstner³

Received: 4 September 2016 / Accepted: 22 May 2017 / Published online: 6 June 2017
© Akadémiai Kiadó, Budapest, Hungary 2017

Abstract The purpose of the presented research is to develop an overall mathematical model, which will allow for a more precise simulation of the operation of a water-to-water heat pump system, having in mind its thermodynamics, fluid mechanics and heat transfer processes. The simulation allows the prediction of the parameters of the state at each and every point of the cycle, i.e., of the heat pump. The developed model is deterministic, stationary and with distributed parameters. The shell and tube heat exchangers' mathematical models are described by coupled differential equations, while the models of the compressor and the expansion valve are described using algebraic equations with lumped parameters. The thermodynamics, fluid mechanics and heat transfer processes are examined as functions of changing mass flow of the cooled water $\dot{m}_{cw} = 0.28, 0.42, 0.55$ and $0.69 [\text{kg s}^{-1}]$, with a referent mass flow of the refrigerant $\dot{m}_{ref} = 0.019 [\text{kg s}^{-1}]$ and the heated water $\dot{m}_{hw} = 0.28 [\text{kg s}^{-1}]$. The used refrigerant is R134a.

Keywords Heat pump · Modeling · Stationary state · Simulation

Abbreviations

A	Area (m^2)
d	Diameter (m)
d_e	Hydraulic diameter (m)
x	Vapor quality (-)
U	Perimeter (m)
G	Mass flux ($\text{kg s}^{-1} \text{m}^{-2}$)
\dot{m}	Mass flow rate (kg s^{-1})
T	Temperature (K)
\bar{T}	Average fluid temperature (K)
f	Friction factor (-)
p	Pressure (Pa)
R	Fluid resistance
\dot{q}	Heat flux (m^{-2})
w	Velocity (m s^{-1})
h	Enthalpy (J kg^{-1})
z	Tube length (m)
v	Specific volume ($\text{m}^3 \text{kg}^{-1}$)
v_h	Spec. volume of function enthalpy ($\text{m}^3 \text{kg}^{-1}$)
v_p	Spec. volume of function pressure ($\text{m}^3 \text{kg}^{-1}$)
Re	Reynolds number (-)
Pr	Prandtl number (-)
X_{tt}	Martinelli parameter (-)
Co	Convection number (-)
C	Characteristic constant of the TEV valve (-)
W	Compressor power (W)

Greek letters

α	Heat transfer coefficient ($\text{W m}^{-2} \text{K}^{-1}$)
λ	Thermal conductivity ($\text{W m}^{-1} \text{K}^{-1}$)
ρ	Density (kg m^{-3})

✉ Sánta Róbert
santar@uniduna.hu

¹ Department of Mechanical Engineering, University of Dunaújváros, Dunaújváros, Hungary

² Department of Building Service and Process Engineering, Budapest University of Technology and Economics, Budapest, Hungary

³ Donát Bánki Faculty of Mechanical and Safety Engineering Institute of Mechanical Engineering and Safety Techniques, Óbuda University, Budapest, Hungary

η Efficiency (-)

Subscripts

ref	Refrigerant
<i>c</i>	Cold
<i>h</i>	Hot
<i>i</i>	In
<i>o</i>	Out
<i>w</i>	Water
liq	Liquid phase
vap	Vapor phase
sh	Superheated
nb	Nucleated boiling
<i>t</i>	Tube wall
eva	Evaporation
con	Condensation
comp	Compressor

Introduction

Increasing the efficiency of energetic processes has been in focus in almost all countries worldwide as modern economies and societies require and use more and more energy. At the same time, problems are accumulating with the use of traditional energy resources, including primarily, expanding detrimental impacts on the environment. The highly significant role of fossil fuels in climate change has been made explicit over the course of the past decade. One tool to firmly restrict this impact is to increase the use of renewable energy resources.

Additionally, to be able to achieve significantly lower impact on the climate, energy consumption has to be reduced to the lowest possible extent [1]. This can be reached by optimizing the energy production and energy use [2].

Taking into account the heating systems in buildings, either in industrial or residential areas, it can be concluded that in the near future substantial changes will occur, meaning that the use of heat pumps, especially compressor-driven heat pumps, will increase considerably [3, 4].

The goal of raising the value of heat pump's coefficient of performance (COP) asks for being able to define as accurately as possible, the structure of the heat pump and the heat pump's processes, i.e., to further develop and refine the physical and mathematical models of these devices.

The experimental investigation of any heat pump's system means a complex problem, mainly due to the financial costs and the large number of variables involved. The use of numerical models can reduce the costs and also facilitate understanding the phenomena related to any

problem [5]. Therefore, the presented research deals with a science-based operational design of compressor-driven water-to-water heat pumps. The introduced mathematical model serves as a simulation tool, which enables the heat pump system's optimization regarding its geometric structure and performance. After a thorough literature review, it can be concluded that current research deals with this topic either partially or by disregarding certain aspects of a stationary water-to-water system when describing its processes [6–19].

In the following Table 1, the results of previous research are presented for the assumed conditions.

The result of the presented literature review points toward a conclusion that researchers carried out a deep and thorough analysis of the heat pump systems of the interest. However, no overall research can be found, which would incorporate all aspects of a stationary water-to-water heat pump system. Therefore, this study aims at contributing to the research by filling the gap in literature with the development of an overall mathematical model, which incorporates the thermodynamics, fluid mechanics and heat transfer processes that occur in heat pumps more precisely than before, taking also into consideration the pressure drop along the heat exchangers by using the momentum equation.

Additionally, the proposed mathematical model allows the prediction of the parameters of the state at each and every point of the cycle, i.e., of the heat pump.

The development of the mathematical model is presented in several steps (Fig. 1):

- Presentation of the system model's structuring with describing the mathematical equations;
- Solution of the suggested mathematical model. For the solution purposes, the solving algorithm is presented. Based on the developed algorithm, the corresponding C++ program is developed as well;
- Validation of the mathematical model by performing a comparison of the simulated results with the measured results, which were presented in the previous research [20].

Mathematical model of the heat pump system

The developed mathematical model's core is represented by the mathematical equation system, which describes the processes in the heat pump. The presented mathematical equations, i.e., the basic equations of the heat exchangers, and the auxiliary equations of the heat exchangers, the equations describing the compressor and the expansion valve, including the initial and boundary conditions, together with the associated dataset, present the overall mathematical model of the heat pump system.

Table 1 Literature review for heat pump models

Author	Year of publication	Compressor	Heat exchangers			Expansion device	Deviation%*
			Pressure drops	Superheating	Heat transfer coefficients		
MacArthur et al. [6]	1989	Polytropic	No	Yes	Variable	Adiabatic Isenthalpic	±5
Stefanuk et al. [7]	1992	Isentropic	No	Yes	Variable	Adiabatic Isenthalpic	Not available
Bourdouxhe et al. [8]	1994	Isentropic	No	No	Assumed constant	Adiabatic Isenthalpic	Not available
Fu et al. [9]	2003	Isentropic	No	Yes	Variable	Adiabatic Isenthalpic	±10
Zhao et al. [10]	2005	Isentropic	No	Yes	Variable	Isenthalpic	Not available
Techarungpaisan et al. [11]	2007	Polytropic	Yes	Yes	Variable	Isenthalpic	$W = \pm 7\%$ $Q_{con} = \pm 24\%$ $Q_{eva} = \pm 21\%$
Belman et al. [12]	2010	Isentropic	No	Yes	Variable	Adiabatic Isenthalpic	±10
Zhenjun et al. [13]	2010	Isentropic	No	Yes	Variable	Isenthalpic	Not available
Kinab et al. [14]	2010	Polytropic	No	Yes	Variable	Adiabatic Isenthalpic	±8
Guo et al. [15]	2011						±10
Choi et al. [16]	2011	Isentropic	No	Yes	Variable	Adiabatic Isenthalpic	±10
Corberan et al. [17]	2011	Isentropic	No	Yes	Variable	Adiabatic Isenthalpic	±5
Ibrahim et al. [18]	2014	Isentropic	No	Yes	Variable	Adiabatic Isenthalpic	±7
Sheng et al. [19]	2015	Isentropic	No	Yes	Variable	Adiabatic Isenthalpic	Not available

* Average difference between simulated and experimental results of the COP values

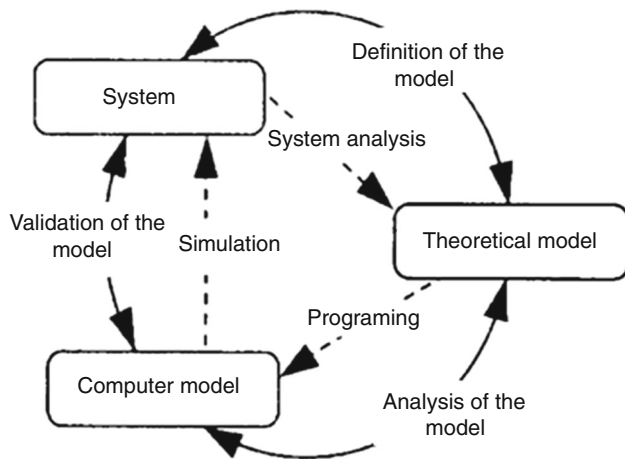


Fig. 1 Modeling and simulation steps

The developed mathematical model is deterministic, stationary and with distributed parameters, with the following assumptions:

- Thermodynamic properties of the lubricant, which flows in the system together with the refrigerant, are not taken into consideration.
- Refrigerant’s flow in the evaporator and the condenser is one dimensional and permanent.
- Refrigerant’s liquid and vapor phases are in thermodynamic equilibrium.

- In heat exchangers, only axial flows are taken into account.

The observed heat exchangers are horizontal, counter-cross flow, shell and tube type. In the current case, the refrigerant flows through in finned tube bundle, while primary and secondary fluids flow in the shell across the tube bundle. In the shell side of the heat exchangers, baffles are applied for supporting the tubes and for inducing cross flow over the tubes, resulting in improved heat transfer performance.

Basic equations of the heat exchangers

The basic equations of the heat exchangers consist of the mass conservation differential equation of the refrigerant (Eq. 1), the momentum conservation equation of the refrigerant (Eq. 2), the energy conservation equations of the refrigerant (Eq. 3), the pipe wall energy conservation equation (Eq. 5) and the water energy conservation equation (Eq. 6) [21].

$$\frac{\partial(\rho \cdot w)}{\partial z} = 0 \rightarrow \rho \cdot w = G = \text{const.} \tag{1}$$

$$\frac{\partial(\rho \cdot w^2)}{\partial z} + \frac{\partial p}{\partial z} + \frac{f_t}{2d_i} \cdot w^2 \cdot \rho = 0. \tag{2}$$

$$\frac{\partial(G \cdot (h + w^2/2))}{\partial z} \pm \dot{q}_i \cdot \frac{U}{A_i} = 0. \tag{3}$$

$$\dot{q}_i = \alpha_{ref} \cdot (T_t - T_{ref}). \tag{4}$$

$$\alpha_{\text{cw}} \cdot d_o \cdot \pi \cdot n \cdot (T_{\text{cw}} - T_t) - \alpha_{\text{ref}} \cdot d_i \cdot \pi \cdot n \cdot (T_t - T_{\text{ref}}) = 0. \quad (5)$$

for: $d_o \cong d_i$

$$\dot{m}_{\text{cw}} \cdot c_{p,\text{cw}} \cdot \frac{dT_{\text{cw}}}{dz} - \alpha_w \cdot d_o \cdot \pi \cdot n \cdot (\overline{T_{\text{cw}}} - \overline{T_t}) = 0. \quad (6)$$

Given the basic equations, several transformations of the basic equations can be performed: based on Eq. 1:

$$w = \frac{G}{\rho} = G \cdot v \rightarrow G = \text{const.}$$

Change in refrigerant's velocity is:

$$\frac{dw}{dz} = G \cdot \frac{dv}{dz}. \quad (7)$$

Change in the refrigerant's specific volume is:

$$\frac{dv}{dz} = \frac{\partial v}{\partial p} \cdot \frac{dp}{dz} + \frac{\partial v}{\partial h} \cdot \frac{dh}{dz},$$

and

$$\frac{dv}{dz} = v_p \cdot \frac{dp}{dz} + v_h \cdot \frac{dh}{dz}. \quad (8)$$

By substituting Eq. 7 into Eq. 8:

$$\frac{dw}{dz} = G \cdot \left(v_p \cdot \frac{dp}{dz} + v_h \cdot \frac{dh}{dz} \right). \quad (9)$$

Based on Eq. 2:

$$G \cdot \frac{dw}{dz} + \frac{dp}{dz} + \frac{f_t}{2d_i} \cdot w^2 \cdot \rho = 0.$$

By applying Eq. 9:

$$G^2 \cdot \left(v_p \cdot \frac{dp}{dz} + v_h \cdot \frac{dh}{dz} \right) + \frac{dp}{dz} + \frac{f_t}{2d_i} \cdot w^2 \cdot \rho = 0.$$

Based on previous transformation, the final form of the momentum conservation equation is:

$$(G^2 \cdot v_p + 1) \cdot \frac{dp}{dz} + G^2 \cdot v_h \cdot \frac{dh}{dz} + \frac{f_t}{2d_i} \cdot w^2 \cdot \rho = 0. \quad (10)$$

By deriving Eq. 3:

$$G^2 \cdot w \cdot \frac{dw}{dz} + G \cdot \frac{dh}{dz} \pm \dot{q}_i \cdot \frac{U}{A_i} = 0.$$

Applying Eq. 1 to the derived Eq. 3 and by applying Eq. 9:

$$G^2 \cdot v \cdot G \cdot \left(v_p \cdot \frac{dp}{dz} + v_h \cdot \frac{dh}{dz} \right) + G \cdot \frac{dh}{dz} \pm \dot{q}_i \cdot \frac{U}{A_i} = 0.$$

Based on previous reasoning, the final form of the energy equation is:

$$G^3 \cdot v \cdot v_p \cdot \frac{dp}{dz} + (G^3 \cdot v_h \cdot v + G) \cdot \frac{dh}{dz} \pm \dot{q}_i \cdot \frac{U}{A_i} = 0. \quad (11)$$

The mathematical model of processes within the heat exchangers is yielded by arranging the equation system consisting of Eqs. 6, 10 and 11 to the derivatives:

$$\frac{dT_{\text{cw}}}{dz} = \frac{\alpha_{\text{cw}} \cdot d_i \cdot \pi \cdot n \cdot (\overline{T_{\text{cw}}} - \overline{T_t})}{\dot{m}_{\text{cw}} \cdot c_{p,\text{cw}}}. \quad (12)$$

$$\frac{dp}{dz} = - \frac{\left(\frac{f_t}{2d_i} \cdot w^2 \cdot \rho \cdot G^2 \cdot v \pm \dot{q}_i \cdot \frac{U}{A_i} \cdot G \right) \cdot v_h + \frac{f_t}{2d_i} \cdot w^2 \cdot \rho}{G^2 \cdot v_p + G^2 \cdot v \cdot v_h + 1}, \quad (13)$$

$$\frac{dh}{dz} = \frac{\left(\frac{f_t}{2d_i} \cdot w^2 \cdot \rho \cdot G^3 \cdot v \pm \dot{q}_i \cdot \frac{U}{A_i} \cdot G^2 \right) \cdot v_p \pm \dot{q}_i \cdot \frac{U}{A_i}}{G \cdot (G^2 \cdot v_p + G^2 \cdot v \cdot v_h + 1)}. \quad (14)$$

Determining the tube's wall temperature from Eq. (5):

$$T_p = \frac{\alpha_{\text{cw}} \cdot T_{\text{cw}} + \alpha_{\text{ref}} \cdot T_{\text{ref}}}{\alpha_{\text{cw}} + \alpha_{\text{ref}}}. \quad (15)$$

The presented equations, supplemented by auxiliary equations, together with the equations of state of the refrigerant and the water, and the equations describing heat exchanger characteristics, comprise the stationary mathematical model of divided characteristics of the evaporator. The systems of Eqs. (12)–(15) are suitable for solution by the Runge–Kutta and Adam–Moulton methods.

Knowing the initial and boundary conditions and by introducing the Δz steps, the equation system gives the thermodynamic and the fluid flow attributes of the water and the refrigerant.

Auxiliary equations of heat exchangers

To be able to solve the basic equations, auxiliary equations are needed as well. The auxiliary equations serve as a correlation toward the determination of the heat transfer coefficients and the pressure drop. However, the existing correlations, which can be found in literature, show great differences [22]. Therefore, parallel to this research, real measurements were carried out to be able to determine the actual heat transfer coefficients both between the refrigerant and the tube, and between the water and the heat exchangers [23, 24]. The results are presented in Table 2.

In the Dittus–Boelter (Eq. 16) correlation, the exponent of Pr should $n = 0.4$ for heating and $n = 0.3$ for cooling, so the correlation is different when it is used in the evaporator and condenser.

The pressure drop distribution in the heat exchangers is also determined based on laboratory measurements [26]. The results are presented in Table 3.

Description of the piston compressor

The compressor as a system component can be described by the enthalpy change specified by the compression ratio and the internal efficiency of the compressor. The output demand of the compressor is this:

$$W = \dot{m}_{\text{ref}} \cdot (h_{\text{con}} - h_{\text{eva}}) \cdot \frac{1}{\eta} \tag{22}$$

Description of the expansion valve

The expansion valve, i.e., the proportioning valve is intended to supply appropriate quantities of refrigerant to the evaporator in function of overheating. Isenthalpic throttling is assumed in operation. The mass flux of the refrigerant flowing through the expansion valve is:

$$G = C \cdot \sqrt{(p_{\text{con}} - p_{\text{eva}}) \cdot \rho_{\text{ref}}} \tag{23}$$

Thermodynamics equations of state of the refrigerant

The thermodynamic and transport properties of the refrigerant are determined by the P - R state equation [27]:

$$p = \frac{R \cdot T}{v - b} - \frac{a(T)}{v \cdot (v + b) + b \cdot (v - b)} \tag{24}$$

with: $a(T) = 0.45724 \cdot \frac{R^2 \cdot T_c^2}{p_c} \cdot \left[1 + \kappa \cdot \left(1 - \sqrt{\frac{T}{T_c}} \right) \right]^2$,

Table 2 Heat transfer coefficient correlations

Region	Refrigerant side heat transfer correlation	Eq.
Single phase [25]	$\alpha_{\text{ref}} = 0.023 \cdot Re^{0.8} \cdot Pr^{0.4} \cdot \frac{\lambda}{d_i}$	(16)
Evaporation [23]	$\alpha_{\text{ref}} = 12.6 \cdot \frac{Co^{0.41}}{X_{tt}^{0.8}} \cdot \alpha_{\text{liq}} + 0.43 \cdot (1 - x) \cdot \alpha_{\text{nb}}$	(17)
Condensation [23]	$\alpha_{\text{ref}} = 28.6 \cdot e^{3.15 \cdot 10^{-5} \cdot Re_c} \cdot Pr^{1.11} \cdot \left(\frac{\lambda}{d_i} \right)$	(18)
Shell side heat transfer correlation		
Single phase [26]	$\alpha_w = 1.66 \cdot Re^{0.43} \cdot Pr^{0.03} \cdot \frac{\lambda}{d_c}$	(19)

Table 3 Pressure drop correlations

Region	Refrigerant side pressure drop correlation	Eq.
Single phase and two phase [26]	$\frac{\Delta p}{\Delta z} = -G^2 \cdot v_{\text{vap}} \cdot \frac{\Delta x}{\Delta Z} - \frac{f_i}{2 \cdot d_i} \cdot G^2 \cdot v_{\text{vap}} \cdot x$	(20)
Shell side pressure drop correlation		
Single phase [26]	$\Delta p = \left(f_i \cdot \frac{\Delta z}{d_c} + 3.09 \right) \cdot \frac{w^2}{2} \cdot \rho$	(21)

$$\kappa = 0.37464 + 1.54226 \cdot \omega - 0.26992 \cdot \omega^2,$$

and $b = 0.07780 \cdot \frac{R \cdot T_c}{p_c}$,

where a and b are energy and size parameters, respectively. R is the universal gas constant. $\omega = 0.3268$ is the acentric factor. Subscript c indicates the critical value.

Solving the mathematical model of the heat pump system

By solving the aforementioned mathematical model, the state changes in the refrigerant and the water can be followed. Considering that the physical model is a distributed parameter model, solving the mathematical model allows for the most detailed monitoring of the thermodynamic and fluid flow attributes in the evaporator and the condenser.

The algorithm for solving the system of equations which defines the heat pump system

The basis of the mathematical modeling, besides the equations, the initial conditions, and the associated data set, comprises of the algorithm of the solution, which also has to be connected and evaluated, since the solving algorithm specifies the accuracy of the solution, as well as the applicability of the model. The simplified block diagram of the algorithm is shown in Fig. 2.

The input data into the simulation is organized in three subgroups:

- Transport properties (thermodynamic and physical properties of the refrigerant, physical properties of water).
- Thermodynamic parameters (water mass flow rate, refrigerant mass flow rate, cold water inlet temperature, temperature of the superheated refrigerant vapor).
- Geometric properties (dimensions of the evaporator and condenser).

The simulation process consists of four sub-processes, which are based on the mathematical models of the compressor, condenser, expansion valve and evaporator. First, the compressor’s mathematical model runs, followed by the condenser’s and expansion valve’s mathematical models. The computation results for the mass flow of the refrigerant in the compressor and the mass flow of the refrigerant in the expansion valve are compared. The temperature of the superheated refrigerant vapor is adjusted until the resulted difference between computation results is smaller than the defined acceptable error. Following this procedure, the evaporator’s mathematical model runs. The computation result output enthalpy from the condenser is compared to the input enthalpy to the evaporator. While the resulted difference between enthalpies is greater than the

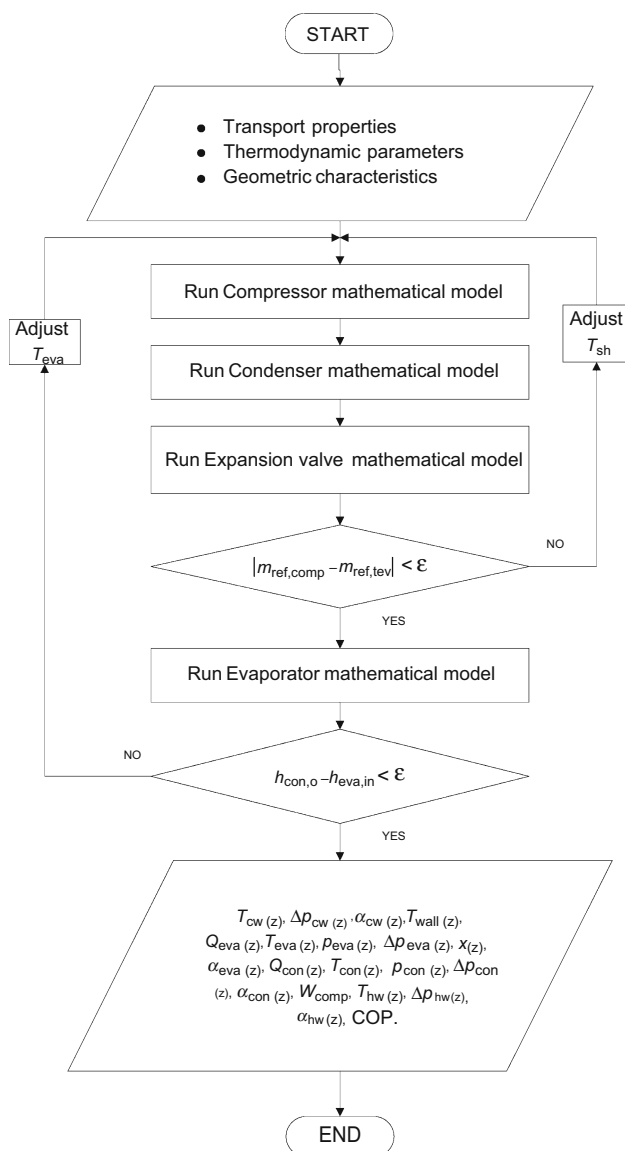


Fig. 2 Simplified algorithm for solving the mathematical model

defined acceptable error, the evaporator's temperature is adjusted, and the procedure is repeated. Following this, an output is generated, which contains the required data for the analysis of the heat pump system.

Presentation of the numerical method applied for solving the mathematical models of system components

The mathematical model of the heat pump system cannot be solved analytically; therefore, numerical simulation has to be applied. Within the numerical simulation, each variable of the model is discretized. This means that each function of independent variables is represented by discrete numbers in a specific breakdown.

In terms of the numerical solution of differential equations, i.e., the equation system, application of the Runge–Kutta method presents a compromise between simplicity and accuracy. This method has been made more precise by applying the Adams–Moulton predictor–corrector method.

The method essentially involves the first four iterations to be performed using Runge–Kutta method in order to provide an input for the Adams–Moulton method. This latter method can be used for the calculation of solutions starting from the fifth iteration. Adams–Moulton's method is an iterative method; the desired level of accuracy can be achieved in the given step, usually by performing iteration several times. The number of iterations is $n < 10$.

The function searched for $F(z) = (p(z), h(z), T(z))$ is a vector function which each component is a function of the distance z from the starting point of the tube ($z = 0$). This means that the calculation of the function F actually involves the calculation of three quantities.

The equation $F' = G(p, h, T, z)$ is to be solved as well.

The Runge–Kutta method is presented as follows:

$$F_{k+1} = F_k + \frac{1}{6} \cdot (k_1 + 2 \cdot k_2 + 2 \cdot k_3 + k_4), \quad (25)$$

where:

$$k_1 = G(p_k, h_k, T_k, z_k), \quad (26)$$

$$k_2 = G\left(p_k + \frac{\Delta}{2} \cdot k_1, h_k + \frac{\Delta}{2} \cdot k_1, T_k + \frac{\Delta}{2} \cdot k_1, z_k + \frac{\Delta}{2}\right), \quad (27)$$

$$k_3 = G\left(p_k + \frac{\Delta}{2} \cdot k_2, h_k + \frac{\Delta}{2} \cdot k_2, T_k + \frac{\Delta}{2} \cdot k_2, z_k + \frac{\Delta}{2}\right), \quad (28)$$

$$k_4 = G(p_k + \Delta \cdot k_1, h_k + \Delta \cdot k_1, T_k + \Delta \cdot k_1, z_k + \Delta), \quad (29)$$

where: p_0, h_0, T_0 are the initial values yielded by the model for $z_0 = 0, k = 0, 1, 2, 3$. Δ is an iteration step. In this case $\Delta = \frac{z}{j}$, where z is the length of the tube, and j is the number of iteration steps.

The Adams–Moulton predictor–corrector method consists of two steps. First, the value of the equation in demand is calculated using the Adams–Bashforth method in the following step:

$$F_{k+1} = F_k + \frac{\Delta}{24} \cdot (55 \cdot G_k - 59 \cdot G_{k-1} + 37 \cdot G_{k-2} - 9 \cdot G_{k-3}), \quad (30)$$

where $G_k = G(p_k, h_k, T_k, z_k)$ and $k \geq 3$ (“predictor” step).

The result obtained is specified by the Adams–Moulton method, generally by running iteration cycles several times (until achieving the desired accuracy; max. 10 in our case). This is the “corrector” step. Formula of the Adams–Moulton method is:

Table 4 Input parameters and initial conditions

Input parameters	
Refrigerant	R134a
Mass flow of refrigerant	$\dot{m}_{ref} = 0.019 [\text{kg s}^{-1}]$
Superheated temperature	$T_{sh} = 4K$
Mass flow of cooled water	$\dot{m}_{cw} = 0.28, 0.42, 0.55$ and $0.69 [\text{kg s}^{-1}]$
Temperature of cooled water	$T_{cw} = 13^\circ\text{C}$
Mass flow of heated water	$\dot{m}_{hw} = 0.28 [\text{kg s}^{-1}]$
Geometrical parameters of heat exchangers	
Shell inner diameter	$d = 42 \cdot 10^{-3} [\text{m}]$
Number of tubes	$n = 5 [pc]$
Tube inner diameter	$d_i = 6 \cdot 10^{-3} [\text{m}]$
Tube outer diameter	$d_o = 8 \cdot 10^{-3} [\text{m}]$
Number of baffles	$r = 15$
Baffle cut	$b = 50\%$
Length of heat exchangers	$z = 3 [\text{m}]$

$$F_{k+1}^{s+1} = F_k^s + \frac{\Delta}{24} \cdot (9 \cdot G_{k+1}^s \cdot + 19 \cdot G_k^s - 5 \cdot G_{k-1}^s + G_{k-2}^s), \tag{31}$$

$s \geq 0, s$ —is the number of steps in the Adams–Moulton method.

Fig. 3 Prediction of the cooled water temperature distribution in the shell side of the evaporator

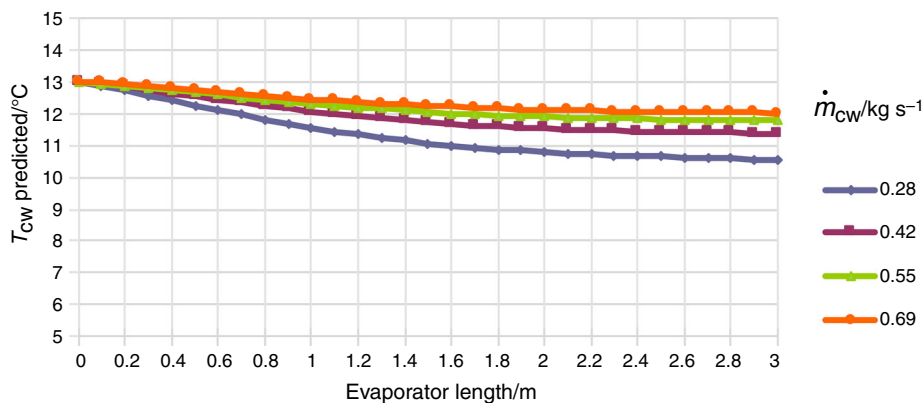
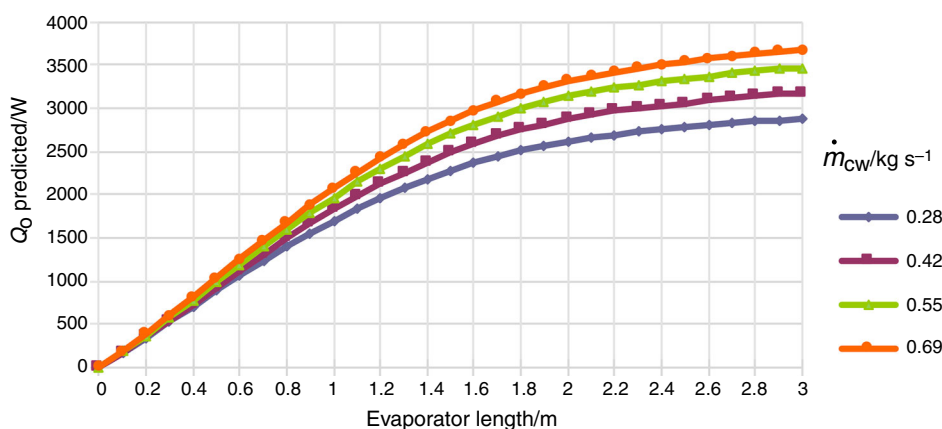


Fig. 4 Prediction of the cooling capacity of the cooled water



The corrector step is canceled in case of $|F_{k+1}^{s+1} - F_{k+1}^s| < \epsilon$ or otherwise after reaching the maximum number of steps ($\epsilon = 10^{-12}, s \leq 10$ in our case). This is followed by the Adams–Bashforth step again by increasing the value of k by one and then by the Adams–Moulton iteration.

Simulation results and discussion

The developed mathematical model is tested by performing a series of numerical simulations to obtain the values for the refrigerant and water regarding their state indicators. The thermodynamics, fluid mechanics and heat transfer processes are examined as functions of changing mass flow of the cooled water ($\dot{m}_{cw} = 0.28, 0.42, 0.55$ and $0.69 [\text{kg s}^{-1}]$). The used input parameters and initial conditions are presented in Table 4.

The simulation results are presented graphically in the following figures (from Figs. 3–15). Additionally to each figure, a short discussion is given regarding the obtained results.

Figure 3 presents the predicted temperature distribution of the cooled water along the shell side of the evaporator.

Fig. 5 Prediction of the heat transfer coefficients in the shell side of the evaporator

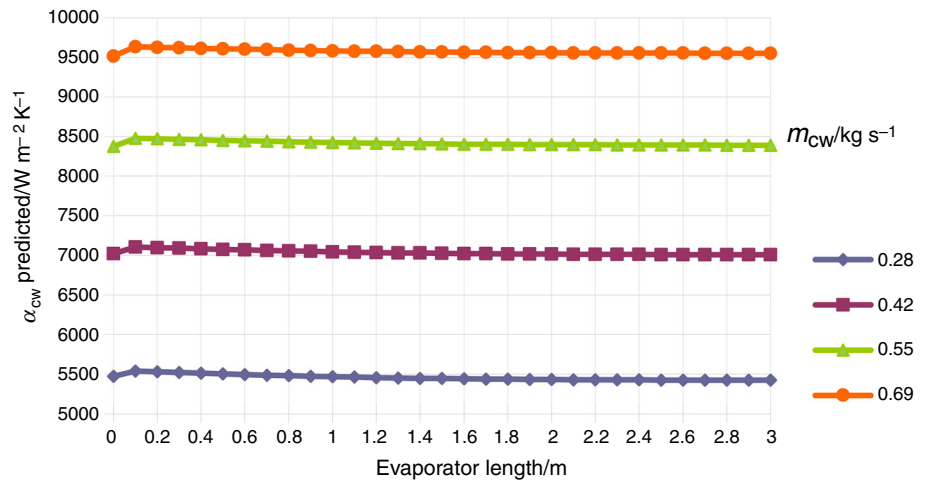


Fig. 6 Prediction of the pressure drop in the shell side of the evaporator

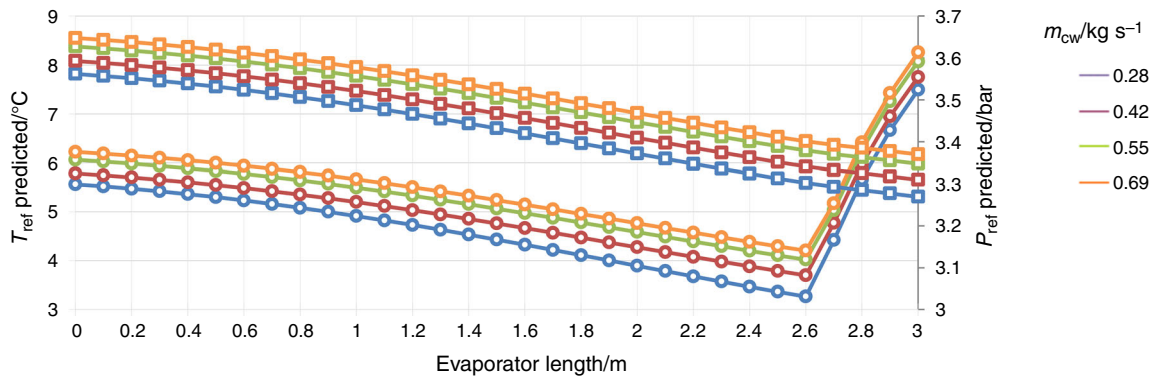
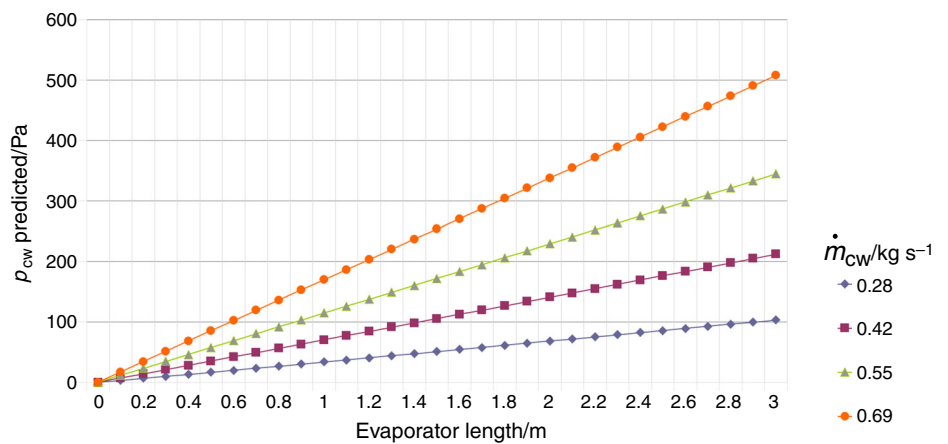


Fig. 7 Prediction of the refrigerant temperature and pressure in tube side of the evaporator

At maximum mass flow levels $\dot{m}_{cw} = 0.69 [\text{kg s}^{-1}]$, the change in the temperature drop is $\Delta T = 1.01 [^{\circ}\text{C}]$. If the mass flow is lowered to 40%, the temperature drop increases to $\Delta T = 2.45 [^{\circ}\text{C}]$.

The cooling capacity of the cooled water along the shell side of the evaporator shows a continuous growth. If the cooled water's mass flow increases, the cooling capacity increases as well (Fig. 4).

Along the shell side of the evaporator, the change in the heat transfer coefficient between the cooled water and the tubes is present but slight. At the same time, the average value of the heat transfer coefficient is significantly changing as a function of the cooled water's mass flow. This is presented in Fig. 5. For higher values of the mass flow, i.e., the higher values of the flow velocity, the heat transfer coefficient show higher values as well, up to 90%.

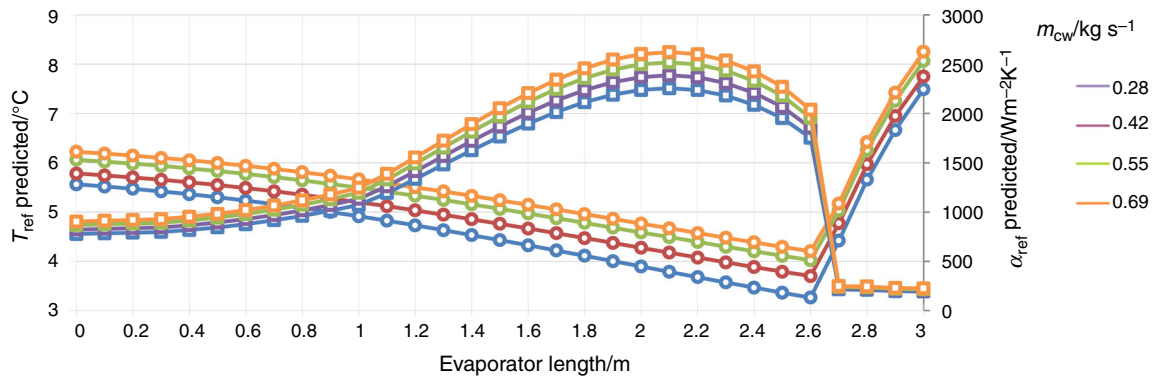


Fig. 8 Prediction of the refrigerant heat transfer coefficients and refrigerant temperature in tube side of the evaporator

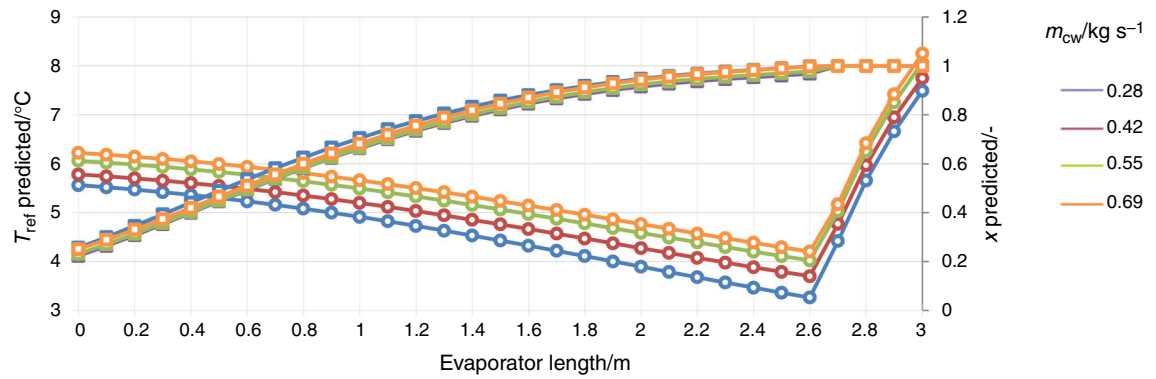


Fig. 9 Prediction of the vapor quality and refrigerant temperature in the tube side of the evaporator

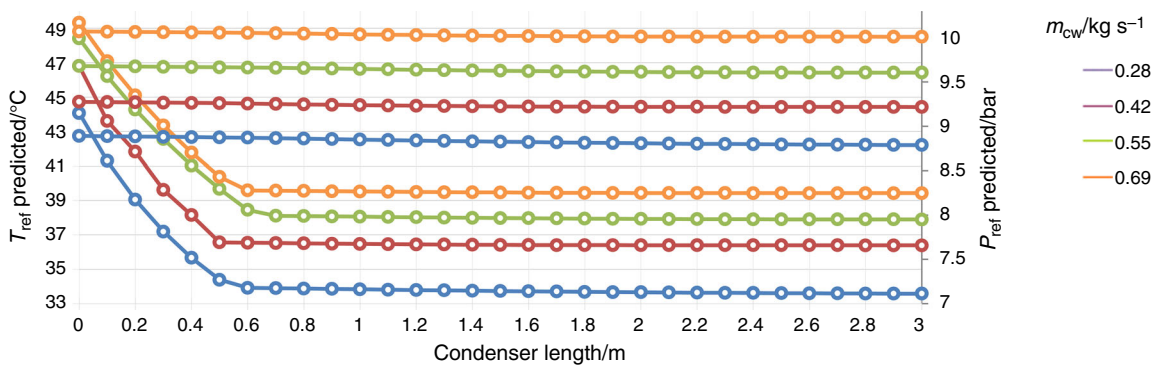


Fig. 10 Prediction of the refrigerant temperature and pressure in tube side of the condenser

In Fig. 6, the cooled water’s pressure drop along the evaporator is presented. The pressure drop is linear. The relation between the pressure drop and mass flow is approximately a quadratic function. However, due to the fact that the flow is not completely turbulent, but in a transition region, instead of $\Delta p = R \cdot v^2$, $\Delta p = R \cdot v^{1.8}$ is suggested.

Figure 7 shows the evaporation completion at a given evaporator’s length, and the refrigerant’s superheating. In addition, the refrigerant’s pressure drop is presented along the evaporator. The pressure drop is almost linear, slightly

convex. If the mass flow is higher, the evaporation pressure increases. Regardless of the mass flow, the pressure drop is always around $\Delta p = 0.28[\text{bar}]$. Due to the pressure drop, the evaporation temperature is not constant. Due to changes in saturation pressure, the saturation temperature changes as well. The temperature change along the evaporation zone is almost $\Delta T = 2.1[^\circ\text{C}]$, regardless of the mass flow value. At the superheating phase, the temperature change is $\Delta T_{\text{sh}} = 4[^\circ\text{C}]$, which represents an input parameter used in the mathematical model.

In Fig. 8, the change in the refrigerant’s heat transfer coefficient in correlation with the temperature is presented along the evaporator. During the two-phase state, i.e., during phase change, the value of the heat transfer coefficient rises significantly. Maximum values can be observed when annular flow is reached, with the vapor quality around $x = 0.8[-]$. The total evaporation occurs at 90% of the evaporator’s surface. After that the vapor phase has low values of heat transfer coefficient, which is very disadvantageous from the heat transfer point of view.

In Fig. 9, the change in the vapor quality in the evaporator is presented in correlation with the temperature. As

already discussed, the total evaporation occurs at 90% of the surface.

In Fig. 10, the refrigerant’s temperature change and pressure drop are presented in the condenser. The refrigerant enters the condenser in a superheated state. At around 30% of the total condenser surface, the saturation temperature is reached. This temperature stays constant during condensation. The pressure drop is lower than in the evaporator. This is due to the fact that here the refrigerant has substantially different thermodynamic parameters than earlier. The Reynolds number and the density have different values.

Fig. 11 Prediction of the refrigerant heat transfer coefficients and the vapor quality in tube side of the condenser

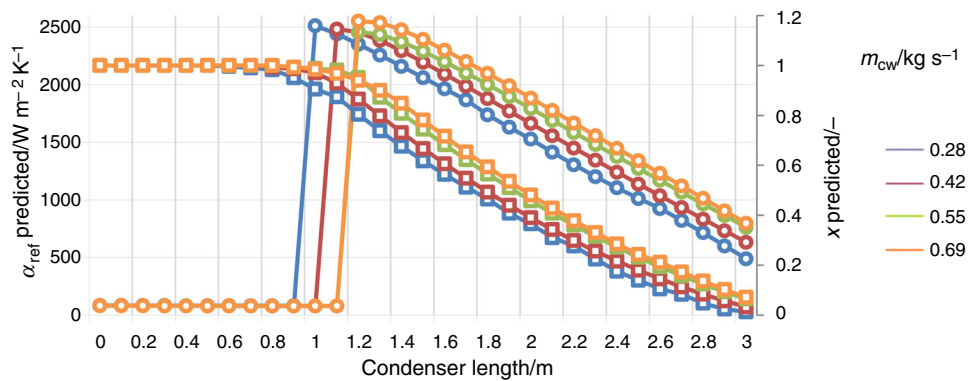


Fig. 12 Prediction of the heat transfer coefficients in the shell side of the condenser

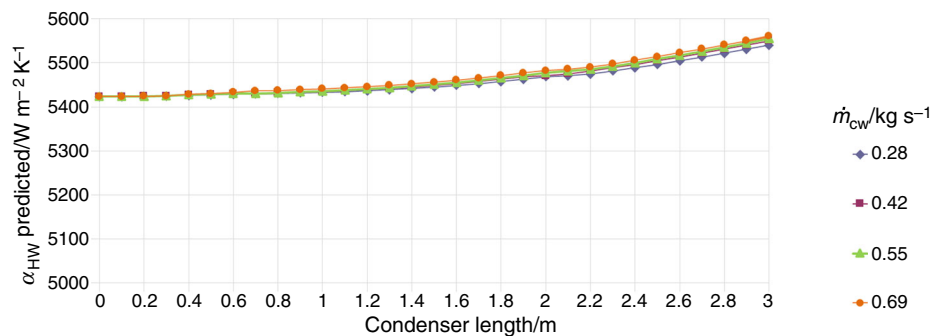


Fig. 13 Prediction of the pressure drop in the shell side of the condenser

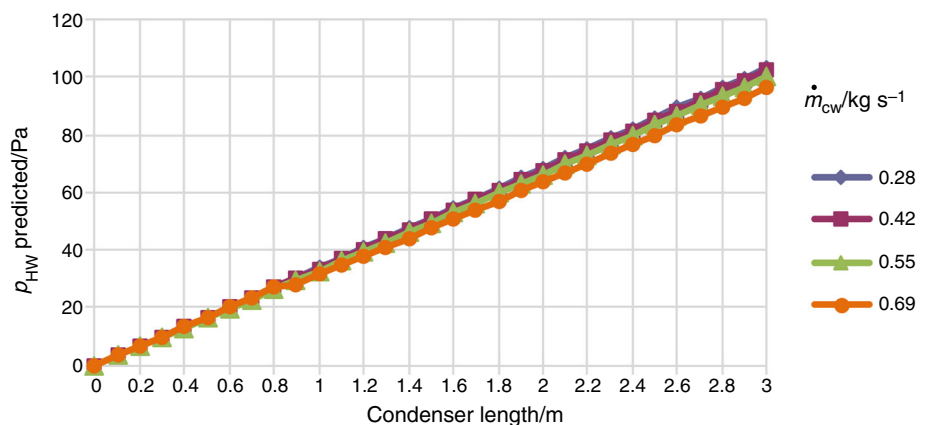


Fig. 14 Prediction of the heating capacity

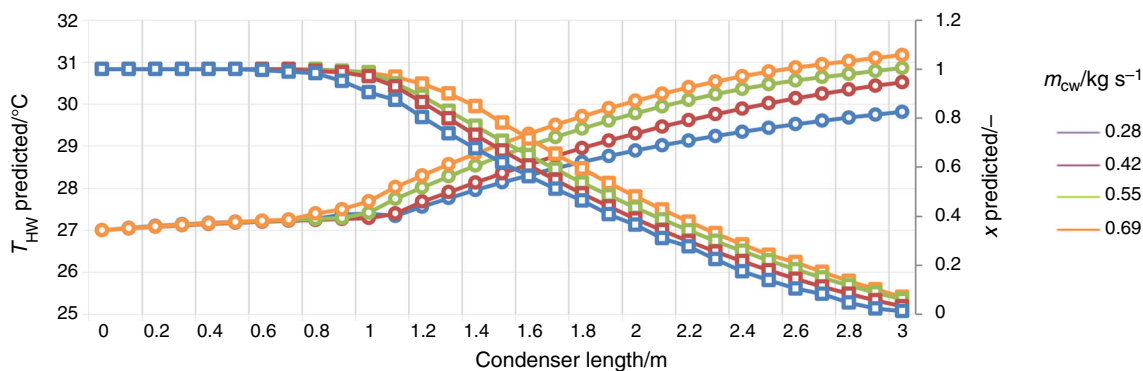
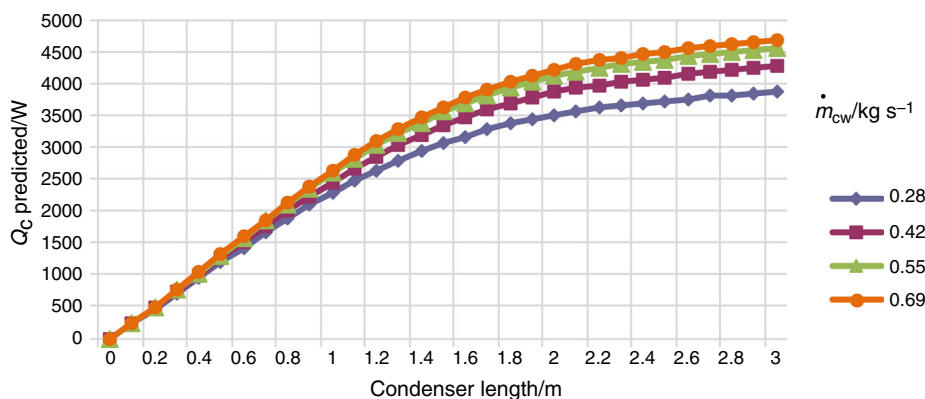


Fig. 15 Prediction of the vapor quality and the heated water temperature in the shell side of the condenser

In Fig. 11, the change in the refrigerant’s heat transfer coefficient and the vapor quality at the tube side of the condenser are presented. The refrigerant transfers the heat at superheated state at the first 30% of the surface. After that, the condensation phase begins. During the two-phase state, a substantial change in the value of the heat transfer coefficient occurs, from $\alpha_{ref} = 81 [W m^{-2} K^{-1}]$ to $\alpha_{ref} = 2512 [W m^{-2} K^{-1}]$. After this change, the value gradually decreases as the liquid phase is more and more present, until the entire vapor is condensed.

In Fig. 12, the change in the heated water’s heat transfer coefficient along the condenser is presented. The value of the heat transfer coefficient shows a slight increase. This is due to slight increase of the temperature along the condenser, as well as the Reynolds number.

In Fig. 13, the pressure drop of the heated water along the condenser is presented. The pressure change is approximately linear. Slight differences in linearity can be observed as a function of temperature change and thus changes in Reynolds number.

In Fig. 14, the change in the heating capacity in the condenser is presented. The heating capacity shows strong increase when the condensation process begins. After this change, the change in the heating capacity in the condenser

gradually decreases as the liquid phase is more and more present.

In Fig. 15, the temperature change in the heated water along the shell side condenser together with the vapor quality is presented. At the first third of the condenser, the temperature change is slight due to low values of heat transfer coefficient. As the condensation prospers, the temperature changes more rapidly.

Conclusions

This paper presents a developed mathematical model for a steady-state compressor-driven water-to-water heat pump. The solution of the presented mathematical model allows the determination of several characteristics of the refrigerant in the cycle, and of the water flowing in the shell side of the evaporator and the condenser, regarding their thermodynamics, fluid mechanics and heat transfer processes.

The presented mathematical model is simulated by changing the mass flow of the cooled water $\dot{m}_{cw} = 0.28, 0.42, 0.55$ and $0.69 [kg s^{-1}]$, with a referent mass flow of the refrigerant $\dot{m}_{ref} = 0.019 [kg s^{-1}]$ and heated water $\dot{m}_{hw} = 0.28 [kg s^{-1}]$. The simulation results show the value

distribution of the parameters of interest along the evaporator and the condenser.

The presented mathematical model is validated through a series of 118 tests [20]. The test results show that an average difference between the modeled and experimental results for the coefficient of performance is 1.73%. The accuracy of the modeled results is determined by the accuracy of heat transfer correlations and pressure drops correlations.

This points toward the conclusion that the proposed mathematical model provides accurate results, i.e., that the parameters of the state for the heat pump are defined with high accuracy, which is the main scientific contribution of this research.

As a result of the developed mathematical model, the compressor-driven water-to-water heat pump's process can be optimized, and the maximum value of COP can be obtained with higher accuracy than before, without the need of building the actual prototype system.

References

- Liu Y, Groll EA, Yazawa K, Kurtulus O. Theoretical analysis of energy-saving performance and economics of CO₂ and NH₃ heat pumps with simultaneous cooling and heating applications in food processing. *Int J Refrig*. 2016;65:129–41.
- Saravanakumar R, Selladurai V. Energy analysis of a domestic refrigerator using eco-friendly R290/R600a refrigerant mixture as an alternative to R134a. *J Therm Anal Calorim*. 2014;115(1): 933–40.
- Rafati M, Kassai M, Ge G, Simonson CJ. Evaluation of defrosting methods for air-to-air heat/energy exchangers on energy consumption of ventilation. *Appl Energy*. 2015;151: 32–40.
- Bagarella G, Lazzarin R, Noro M. Sizing strategy of on-off and modulating heat pump systems based on annual energy analysis. *Int J Refrig*. 2016;65:183–93.
- Kóvári A. Effect of leakage in electrohydraulic servo systems based on complex nonlinear mathematical model and experimental results. *Acta Polytech Hung*. 2015;12(3):129–46.
- MacArthur JW, Grald EW. Unsteady compressible two-phase flow model for predicting cyclic heat pump performance and a comparison with experimental data. *Int J Refrig*. 1989;12:29–41.
- Stefanuk NBM, Aplevich JD, Renksizbulut M. Modeling and simulation of a superheat-controlled water-to-water heat pump. *ASHRAE Trans*. 1992;98(2):172–84.
- Bourdouxhe JPH, Grodent M, Lebrun JJ, Saavedra C, Silva KL. A toolkit for primary HVAC system energy calculation—part 2: reciprocating chiller models. *ASHRAE Trans*. 1994;100(2): 774–86.
- Fu L, Ding G, Zhang C. Dynamic simulation of air-to-water dual-mode heat pump with screw compressor. *Appl Therm Eng*. 2003;23:1629–45.
- Zhao L, Zaheeruddin M. Dynamic simulation and analysis of a water chiller refrigeration system. *Appl Therm Eng*. 2005;25: 2258–71.
- Techarungpaisan P, Theerakulpisut S, Priprem S. Modeling of a split type air conditioner with integrated water heater. *Energy Convers Manag*. 2007;48:1222–37.
- Belman JM, Navarro-Esbri J, Ginestar D, Milian V. Steady-state model of a variable speed vapor compression system using R134a as working fluid. *Int J Energy Res*. 2010;34:933–45.
- Zhenjun X, Huaizhi W, Meiling W. Energy performance and consumption for biogas heat pump air conditioner. *Energy*. 2010;35:5497–502.
- Kinab E, Marchio D, Riviere P, Zoughaib A. Reversible heat pump model for seasonal performance optimization. *Energy Build*. 2010;12:2269–80.
- Guo JJ, Wu JY, Wang RZ, Li S. Experimental research and operation optimization of an air-source heat pump water heater. *Appl Energy*. 2011;88:4128–38.
- Choi JW, Lee G, Kim MS. Numerical study on the steady state and transient performance of a multi-type heat pump system. *Int J Refrig*. 2011;34:429–43.
- Corberan JM, Galvan IM, Ballester SM, Macia JG, Pastor RR. Influence of the source and sink temperatures on the optimal refrigerant charge of a water-to-water heat pump. *Int J Refrig*. 2011;34:881–92.
- Ibrahim O, Fardoun F, Younes R, Gualous HL. Air source heat pump water heater: dynamic modeling, optimal energy management and mini-tubes condensers. *Energy*. 2014;64:1102–16.
- Sheng Y, Zhang Y, Zhang G. Simulation and energy saving analysis of high temperature heat pump coupling to desiccant wheel air conditioning system. *Energy*. 2015;83:583–96.
- Santa R, Garbai L, Fürstner I. Optimization of heat pump system. *Energy*. 2015;89:45–54.
- Szlivka F. Different mathematical solutions on gas oscillation. *Acta Polytech Hung*. 2014;11(02):101–15.
- Santa R. The analysis of two-phase condensation heat transfer models based on the comparison of boundary condition. *Acta Polytech Hung*. 2012;9(6):167–80.
- Santa R, Garbai L. Measurement testing of heat transfer coefficients in the evaporator and condenser of heat pumps. *J Therm Anal Calorim*. 2015;119:2099–106.
- Ali ShB, Hameed BM, Alasdair NC, Anthony JG. Measuring the average direct contact heat transfer coefficient of a liquid–liquid–vapour direct contact heat exchanger. *Appl Therm Eng*. 2016; 103:47–55.
- Dittus FW, Boelter LMK. Heat transfer in automobile radiators of the tubular type. *PublEng*. 1930;2:443.
- Santa R. Simulation and optimisation of compressor driven heat pumps for building services. Hungary: Department of Building Service Engineering and Process Engineering. Ph.D. Budapest University of Technology and Economics Faculty of Mechanical Engineering; 2014.
- Alexander DJ, Libretto SE. An overview of the toxicology of HFA-134a (1,1,1,2-tetrafluoroethane). *Hum Exp Toxicol*. 1995;14(9):715–20.